Dynamics of the N(2 D) + D 2 Reaction from Crossed-Beam and Quasiclassical Trajectory Studies †

ARTICLE *in* THE JOURNAL OF PHYSICAL CHEMISTRY A · FEBRUARY 2001

Impact Factor: 2.69 · DOI: 10.1021/jp0036238

7 AUTHORS, INCLUDING:

Nadia Balucani
Università degli Studi di Perugia
162 PUBLICATIONS **3,461** CITATIONS
SEE PROFILE

Michele Alagia
Italian National Research Council
146 PUBLICATIONS **2,003** CITATIONS
SEE PROFILE

Laura Cartechini
Italian National Research Council
68 PUBLICATIONS **1,433** CITATIONS
SEE PROFILE

Piergiorgio Casavecchia
Università degli Studi di Perugia
168 PUBLICATIONS **4,307** CITATIONS
SEE PROFILE

Dynamics of the N(^{2}D) + D_2 Reaction from Crossed-Beam and Quasiclassical Trajectory Studies†

Nadia Balucani, Michele Alagia,‡ Laura Cartechini, Piergiorgio Casavecchia,*,§ and Gian Gualberto Volpi

Dipartimento di Chimica, Università di Perugia, 06123 Perugia, Italy

Lisa A. Pederson and George C. Schatz*

Department of Chemistry, Northwestern University, Evanston, Illinois 60208-3113

Received: October 3, 2000; In Final Form: January 8, 2001

The dynamics of the prototypical insertion reaction N(^{2}D) + D_2 have been investigated in a combined experimental and theoretical study. Angular and velocity distributions of the ND product have been obtained in crossed molecular beam experiments with mass spectrometric detection at two collision energies (E_c = 3.8 and 5.1 kcal mol^{-1}). The center-of-mass product angular and translational energy distributions have been derived; at both E_c's, the former is found to be nearly backward−forward symmetric, reflecting an insertion dynamics, and the latter corresponds to a fraction of total available energy released in translation of 32%, indicating that the ND product is highly internally excited. Quasiclassical trajectory (QCT) calculations were performed on an accurate potential-energy surface obtained from large-scale ab initio electronic structure computations, and the results were compared to experiment. Generally good agreement was found between the experimental results and the theoretical predictions; however, small, yet significant, discrepancies point to some inaccuracy of the QCT treatment, calling for a quantum scattering study of the title reaction.

I. Introduction

Chemical reactions of nitrogen atoms with inorganic and organic molecules are significant in a wide variety of systems: earth-orbital environment, planetary and extraplanetary atmospheres, interstellar and circumstellar clouds, hydrocarbon air combustion, and charged particle collisions.[1,2] The study of N atom reactions has always represented a challenge to chemists. Traditionally, these reactions were investigated using "active nitrogen"[3−6] and the reaction mechanism speculated from early product analysis; in those studies, the only reactive species was assumed to be the ground state of atomic nitrogen, N(^{4}S).[6,7] More recent and accurate rate constant measurements[8] have established that, when the reactive partner is a closed shell molecule, in most cases the reactivity of the ground state ^{4}S is practically negligible, whereas the first electronically excited metastable state ^{2}D (whose energy content is 55.1 kcal mol^{-1} with respect to the ground state) was found to be the most reactive low-lying state of atomic nitrogen.

A deeper understanding of chemical reactions is provided by reaction dynamics studies. Only recently, the experimental investigation of N(^{2}D) reactions at the microscopic level has become possible. Important reactions such as N(^{2}D) + O_2, thought to be responsible of the anomalously large concentration of NO (nitric oxide) in the upper atmosphere,[9] can now be tackled, as well as reactions of N(^{2}D) with simple hydrocarbons,[10,11] of great relevance in the atmosphere of Saturn's moon Titan.[12]

In this paper, we report experimental and theoretical results on the dynamics of the simplest N(^{2}D) reaction, that with molecular hydrogen

$$N(^2D) + H_2(^1\Sigma_g^+) \rightarrow NH(X^3\Sigma^-) + H(^2S) \qquad \Delta H^\circ_0 = -33.2 \text{ kcal mol}^{-1} \quad (1)$$

Specifically, by carrying out crossed molecular beam (CMB) experiments, we have derived reactive double differential cross sections (DCSs), and by using quasiclassical trajectory (QCT) methods, we have computed the dynamics on a recently developed doublet ground-state potential-energy surface (PES) of NH_2.[13] By combining experimental findings and theoretical predictions, a clear insight into the micro-mechanism has been gained for the first time on an N(^{2}D) reaction.

The reason for focusing our attention on this reactive system is that not only does it represents a prototypical case (because of its relative simplicity) for understanding the chemical behavior of atomic nitrogen in the ^{2}D state but it is also a useful prototype for a more general understanding of the class of reactions usually termed as *insertion* reactions. The synergism between experiment and theory in the field of reaction dynamics has, indeed, resulted in detailed comparisons between state-of-the-art experiment and state-of-the-art theory for the dynamics of benchmark three-atom reactions (H + H_2, F + H_2, and Cl +

† Part of the special issue "Aron Kuppermann Festschrift". It is a great pleasure and most appropriate to dedicate, on the occasion of his 75th birthday, this paper to Professor Aron Kuppermann, the pioneer and inspirer of quantum scattering studies on the dynamics of elementary chemical reactions that have stimulated a great amount of experimental dynamics work over the past 30 years.

* To whom correspondence should be addressed. Piergiorgio Casavecchia, Dipartimento di Chimica, Università di Perugia, Via Elce di Sotto, 8, 06123 Perugia, Italy. E-mail: piero@dyn.unipg.it. Tel: +39 075 585 5514. Fax: +39 075 585 5606. http://www.chm.unipg.it/chimgen/mb/exp3/casavecchia.html

‡ Present address: INFM, Sincrotrone Elettra. 34012, Trieste, Italy.

§ Visiting Miller Professor, Department of Chemistry, University of California, Berkeley.

10.1021/jp0036238 CCC: $20.00
Published on Web 02/20/2001

H_2, together with their isotopic variants), which all belong to the class of *abstraction* reactions (for a review of recent work see ref 14). At the same time, a new effort has been directed toward the combined experimental and theoretical investigation of the more complex family of insertion reactions,[14−20] which usually involve electronically excited atoms, as the important species O(^{1}D), and occur on multiple PESs including nonadiabatic effects. The reaction O(^{1}D) + H_2 → OH + H has long served as the prototypical insertion reaction,[14−17] but other systems such as S(^{1}D) + H_2,[18] C(^{1}D) + H_2,[19] and the title reaction[20] have recently added to the list of insertion reactions for which DCSs have been measured and for which theoretical study is within the capabilities of modern computers.[13,20−23] The common characteristics of these reactions is that they occur on PESs with a deep potential well between reactants and products associated with a strongly bound species (H_2O, H_2S, CH_2, and NH_2) which is formed following the insertion of the excited atom into the H−H bond. Because of the stability of the intermediate with respect to reactants and products, these insertion reactions are often assumed to proceed statistically. Nevertheless, the formation of a light, highly excited intermediate with few internal degrees of freedom seems to alter this simplistic prediction in many cases. Indeed, O(^{1}D) + H_2 is often considered to be a textbook case of this behavior, as experimental product distributions point to nonstatistical behavior.[14,16] However, an additional abstraction pathway involving excited surfaces[15] is also available for that system, and therefore, it is not clear what the origin of the nonstatistical energy partitioning is.

Cleaner cases of insertion reactions appear to be the two reactions S(^{1}D) + H_2 and C(^{1}D) + H_2, which occur only on the lowest PES and are both weakly exoergic ($\Delta H°_0 \sim -6$ to + 7 kcal mol^{-1}). These two reactions have been found to behave nearly statistically, because a simple phase space theory (PST) model was able to give a fair description of the product translational energy distribution.[18,19] Nevertheless, significant discrepancies were noted for angular distributions, and therefore, a definite assessment of the reaction mechanism will be given only when scattering calculations on chemically accurate PESs suitable for dynamical studies are performed. Very recently Skodje and co-workers[23] have derived a PES and run QCT trajectories for the S(^{1}D) + H_2 (and isotopic variant) reactions. The comparison with the experimental DCSs and excitation functions determined by Liu and co-workers points to some nonstatistical effects also for this system.[23]

Different from the above-mentioned insertion reactions, which are all barrierless and almost gas-kinetic, the N(^{2}D) + H_2 reaction is characterized by an activation energy of 1.7 kcal mol^{-1} (1.9 kcal mol^{-1} in the case of the N(^{2}D) + D_2 reaction), as derived from rate constant measurements in the range T = 213−300 K.[24a] The room-temperature rate constants have been determined to be 2.3×10^{-12} and 1.4×10^{-12} cm^3 molecule^{-1} s^{-1} for the reaction with H_2 and D_2, respectively.[24] Early infrared chemiluminescence measurements performed by Dodd and co-workers[25] of the nascent NH vibrational population from the N(^{2}D) + H_2 reaction pointed to a behavior which is similar to that of O(^{1}D) + H_2 as far as the product energy release is concerned,[16] with an NH vibrational population hotter than that of the statistical one. From these first observations, it was suggested that a direct H atom collinear−abstraction mechanism rather than an insertion complex−formation mechanism dominates the reaction.[25] These findings were then supported by dynamical calculations on a first PES, derived from ab initio molecular orbital calculations (first-order configuration interaction).[26] This first surface was characterized by a barrier for collinear approach lower than that for insertive attack, thus favoring the abstraction mechanism; the measured hot vibrational distribution was well reproduced by QCT and approximate quantum calculations.[26] More recently, from laser-induced fluorescence (LIF) measurements of the nascent internal population of NH/ND (v' = 0 and 1), Umemoto and co-workers[27] have found a broad product rotational distribution, in contrast to the strongly inverted one observed for OH(OD) products from the O(^{1}D) + H_2/D_2 reactions.[16c,g] Interestingly, in a recent off-diagonal LIF study,[28] the NH vibrational distribution was found to be colder than that derived[25] from the infrared emission measurements.

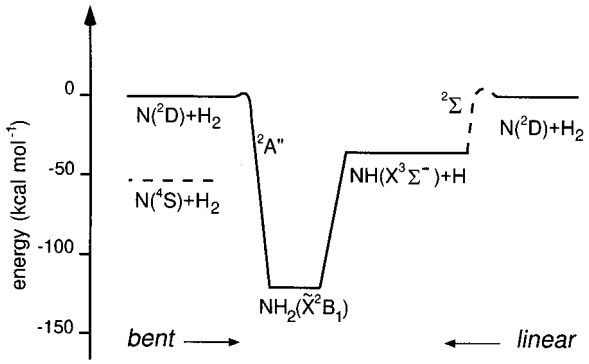

Figure 1. Schematic energy level and correlation diagram for the reaction N(^{2}D) + H_2 based on ab initio electronic structure calculations of the ground PES. Both bent and linear geometries are shown.

The initial suggestion that the dominant reaction pathway is direct abstraction was definitely questioned in previous work from our laboratory[20] on the isotopic variant N(^{2}D) + D_2 → ND + D, because the differential cross section was found to be backward−forward symmetric at the collision energy (E_c) of 5.1 kcal mol^{-1}. The scattering results were presented together with calculations of an accurate ab initio ground-state PES for NH_2 and QCT studies.[20]

The new PES[13] pointed to the dominance of the C_{2v} insertion mechanism over the collinear abstraction mechanism, in contrast to the previous PES.[26] The calculated saddle-point energy for the perpendicular approach was found to be 1.9 and 2.3 kcal mol^{-1} for the second-order configuration interaction (SOCI) surface with and without including the Davidson correction, respectively. On the same PES, the collinear stationary point energy was calculated to be 5.5 kcal mol^{-1} (4.6 kcal mol^{-1} when including the Davidson correction) and the intermediate well energy was found to be −126.4 kcal mol^{-1} (−125.5 kcal mol^{-1} when including the Davidson correction), which compares well with the experimental value of −124.5 kcal mol^{-1} (see Figure 1 for a simplified scheme of the ground-state PES). We have to note that the thermal rate constant was not well reproduced by QCT calculations on the new PES, which gave a value about a factor 3 lower than that of the experiment.[13] This suggested that the calculated barrier is probably too high or that quantum effects play a role. Also, another reason could be that a significant contribution to the reaction is provided by one of the four excited electronic state surfaces, for example, the $1^2A'$ state surface, for which ab initio calculations[21] have found a barrier of 3.4 kcal mol^{-1}. This possibility has been extensively explored in recent theoretical work[21] and it was found that the excited state contribution is about 12% of the ground state one, thus improving only a little the comparison with the experimental thermal rate constants.[27] Exact quantum mechanical (QM) scattering calculations[22] on the ground state ab initio PES (including the Davidson correction) have also been performed

and cross sections derived for $N(^2D) + H_2$ ($v = 0$, $j = 0$) at E_c = 1.6, 2.5, and 3.8 kcal mol^{-1}. As might be expected for a reaction with a barrier, the QM results (restricted to the initial H_2 rotational level $j = 0$) give total reactive integral cross sections (ICS) systematically larger than the QCT ones, with the difference increasing as the collision energy decreases (at 1.6 kcal mol^{-1} the QM total ICS is about four times larger than the QCT one). The distribution of final rovibrational states was also found to have a more statistical nature than that derived from QCT calculations. The QM DCSs were almost backward−forward symmetric with a slight preference for forward scattering at $E_c = 2.5$ kcal mol^{-1} and for backward scattering at E_c = 3.8 kcal mol^{-1}; also, the degree of polarization is higher than that derived from QCT calculations and from experimental results (on $N(^2D) + D_2$). Very recently, the QM calculations were carried out also for initial $j = 1$ and 2 of H_2 at $E_c = 3.8$ kcal mol^{-1}, and the result was that the total angular distribution is essentially symmetric when averaged over the reactant rotational distribution.[29] The origin of these differences between classical and quantum results has not been studied, but some aspects of it may be due to tunneling through the centrifugal (and also potential) barrier. These differences are mostly rather subtle, so the QCT results still provide a useful guide for interpreting the experiment.

In this paper, we extend the comparison of experimental results and QCT predictions for the $N(^2D) + D_2$ reaction to a second collision energy of 3.8 kcal mol^{-1}. Also, because the reported QCT calculations at $E_c = 5.1$ kcal mol^{-1} were previously performed on the PES derived without including the Davidson correction,[20] the differential cross section calculated on the PES where the Davidson correction has been taken into account will be compared to experimental results.

The paper is organized as follows. In section II, the experimental method is briefly described and the experimental results and data analysis are reported. In section III, details of the QCT calculations are given. Experimental results and theoretical predictions are compared in section IV. The Discussion and the Conclusion are presented in section V and VI.

II. Experimental Results and Analysis

A. The CMB Experiments. The scattering experiments were carried out by using a CMB apparatus that has been described in detail elsewhere.[30,31] Briefly, two well collimated supersonic beams of the reagents are crossed at 90° in a large scattering chamber with background pressure in the 10^{-7} mbar range, which ensures the single collision conditions. The detection system consists of an electron bombardment ionizer, a quadrupole mass filter, and an off-axis (90°) secondary electron multiplier. The ionizer is located in the innermost region of a triply differentially pumped ultrahigh-vacuum chamber which is maintained in the 10^{-11} mbar pressure range in operating conditions by extensive ion, turbo, and cryo pumping. The whole detector unit can be rotated in the collision plane around an axis passing through the collision center, and the velocities of the particles can be derived from time-of-flight (TOF) measurements. In the present experiments, a selection of the velocities as well as a partial selection of the internal quantum states of the reactants by supersonic expansion is achieved. The measurement of the translational energy of the products also gives (by energy conservation) their internal (rotational and vibrational) energy. The two beam sources are usually doubly differentially pumped; to gain intensity, however, for the present experiment, the secondary molecular beam source was brought closer to the collision region, with only one stage of differential pumping.

The study of the title reaction has been particularly challenging because of the unfavorable N isotopic distribution and of the high inherent background at $m/e = 16$ (because of CH_4) in any UHV chamber. This combination forced us to use isotopically labeled ^{15}N and $^2H_2$, which allowed us to detect the ND product at the mass-to-charge (m/e) ratio of 17 and to achieve a sufficiently good signal-to-noise ratio, although the reactive cross section is relatively small. The supersonic atomic nitrogen beams were generated by the high-pressure radio frequency (RF) discharge beam source successfully used in our laboratory over a number of years to generate intense supersonic beams of atoms and radicals.[14,32−34] The RF source, which is similar in design to that originally developed by Sibener et al.[35] for atomic oxygen production, has been discussed in some detail elsewhere.[31,32] Briefly, high levels of RF power are fed, through an LC circuit made to resonate around 14 MHz, into a plasma contained in a quartz nozzle (orifice diameter 0.26 mm in the present setup) cooled with low electrical conductivity water. The plasma is directly localized behind the orifice of the nozzle, which permits achieving a high degree of molecular dissociation. The beam is skimmed by a boron nitride skimmer (diameter 1.0 mm) located at a distance of 5.2 mm from the nozzle and further collimated by a rectangular slit. From dilute (2.5%) mixtures of N_2 (50% isotopically enriched in $^{15}N_2$) in He, a high degree of molecular dissociation (∼60%) was achieved. Atomic nitrogen was produced in a distribution of electronic states which has been characterized by Stern−Gerlach magnetic analysis:[32] 72% of the N atoms were found in the ground ^4S state and 21% and 7% in the metastable excited ^2D and ^2P states (lying 55.1 and 82.1 kcal mol^{-1}, respectively, above the ground state). The use of nitrogen atom beams which contain, in addition to $N(^2D)$, also $N(^4S)$ and $N(^2P)$ does not represent a complication in the present studies because the reaction of $N(^4S)$ with H_2 is strongly endoergic ($\Delta H°_0 = 21.7$ kcal mol^{-1}) and that of $N(^2P)$ about 2 orders of magnitude slower ($k_{298} = 1.4 \times 10^{-14}$ cm^3 molecule^{-1} s^{-1})[24a] than that of $N(^2D)$. In addition, the extent of the product translational energy release confirms that the measured ND product is all coming from the $N(^2D)$ reaction. In the lower energy experiment, the atomic nitrogen beam was obtained by discharging 200 mbar of the N_2/He mixture at 200 W; a peak velocity of 2597 m s^{-1} and a speed ratio of 7.3 were obtained. Slightly different conditions were used for the higher energy experiment: by discharging 235 mbar at 250 W, a peak velocity and speed ratio of 2579 m s^{-1} and 8.0 were obtained. The angular divergence was 2.3° in both cases.

The beam of D_2 was produced by supersonic expansion through a 70 μm stainless steel nozzle of *normal* (n) D_2, at a stagnation pressure of 3.5 bar and room temperature for the lower energy experiment and at a pressure of 4 bar with the nozzle resistively heated at 573 K (in order to increase the beam translational energy) for the higher energy experiment. Peak velocity and speed ratio were 1896 m s^{-1} and 14.6 and 2579 m s^{-1} and 15.3, respectively, in the two cases. With only one stage of differential pumping, the beam angular divergence was about 5°. The rotational temperatures of the n $D_2(j)$ reagent molecules in the beams under the expansion conditions were estimated by extrapolating the consistent experimental determinations of Pollard et al.[36] to be 140 and 290 K. The relative rotational state populations are 0.37, 0.30, 0.29, and 0.04 and 0.19, 0.21, 0.39, and 0.21 for $j = 0$, 1, 2, and ≥3, respectively, for the lower and the higher energy experiment. We recall that the rotational energies of the $j = 1$, 2, and 3 states of D_2 with respect to $j = 0$ are 0.17, 0.51, and 1.03 kcal mol^{-1}.

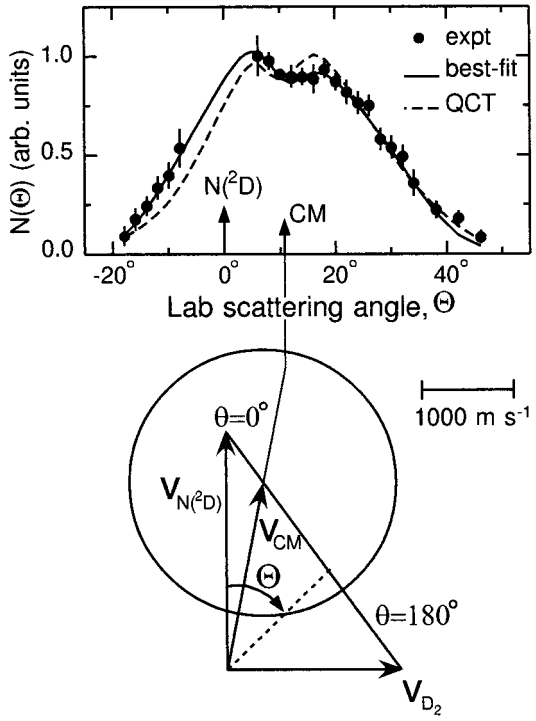

Figure 2. Laboratory ND angular distribution from the N(^{2}D) + D_2 reaction at $E_c = 3.8$ kcal mol^{-1} and the corresponding Newton diagram showing the kinematics of the experiment. Solid line: calculated curve when using the best-fit CM angular and translational energy distributions. Dashed line: calculated curve when using the QCT derived CM angular and translational energy distributions.

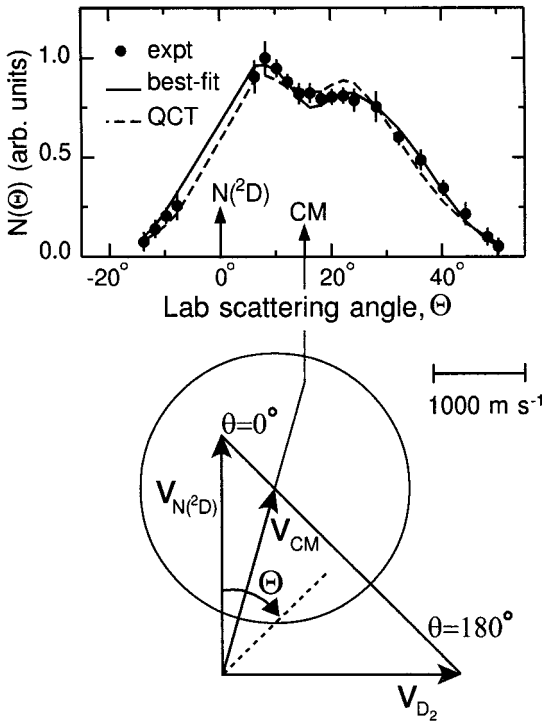

Figure 3. As in Figure 2, but at $E_c = 5.1$ kcal mol^{-1}.

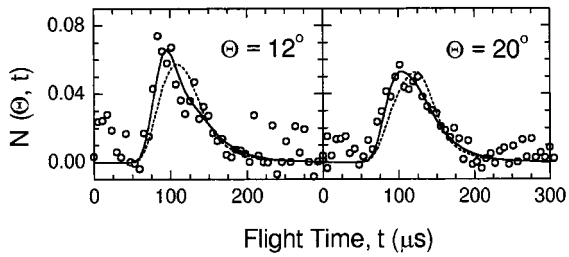

Figure 4. TOF spectra of the ND product from the N(^{2}D) + D_2 reaction at $E_c = 3.8$ kcal mol^{-1}. Solid and dashed lines as defined in Figure 2.

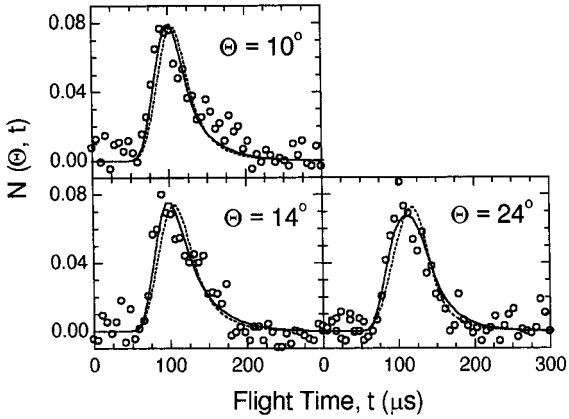

Figure 5. TOF spectra of the ND product from the N(^{2}D) + D_2 reaction at $E_c = 5.1$ kcal mol^{-1}. Solid and dashed lines as defined in Figure 2.

The laboratory angular distributions of the ^{15}ND product $N(\Theta)$ were obtained by taking several scans of 50 s counts at each angle. The nominal angular resolution of the detector for a point collision zone is 1°. The secondary target beam (D_2 beam) was modulated at 160 Hz by a tuning fork chopper. The background and signal-plus-background counts are obtained from a pulse counting dual scaler, synchronously gated with the tuning fork.

The reactant beam velocities are measured by single-shot TOF analysis using a standard disk (four slits, 0.3 mm wide on a 145 mm diameter disk, thickness 0.1 mm, 300 Hz), located at the entrance of the detector and positioning the detector (equipped with a 0.3 mm diameter entrance slit) in axis with the beam. Product velocity distributions $N(\Theta,v)$ were obtained at a few selected laboratory angles using the cross-correlation TOF technique:[37] a pseudorandom chopper (145 mm diameter, 0.1 mm thick) with four 127-bit pseudorandom sequences (hole width about 0.9 mm) was spun at 328.1 Hz corresponding to a dwell time of 6 μs/channel. For the TOF measurements, a high-speed multichannel scaler and a computer-controlled CAMAC data acquisition system was used. The flight length was 24.5 cm. Counting times were of 60 min.

The laboratory product angular distributions from the ^{15}N-(^{2}D) + D_2 reaction at $E_c = 3.8$ and 5.1 kcal mol^{-1} are shown in Figures 2 and 3 together with the canonical Newton diagrams. The error bars are indicated representing ± 1 standard deviation. The solid and dashed curves are best-fit and QCT calculations, respectively, as described in section II.B and III. The TOF distributions at selected laboratory angles are shown in Figures 4 and 5.

B. Analysis of the Experimental Results. For the physical interpretation of the scattering results, it is necessary to transform the angular $N(\Theta)$ and velocity $N(\Theta,v)$ distributions measured in the laboratory (LAB) coordinate system to the center-of-mass (CM) reference frame. This transformation is fairly straightforward, and the relation between LAB and CM fluxes is given by

$$I_{LAB}(\Theta,v) = I_{CM}(\theta,u)v^2/u^2$$

i.e., the scattering intensity observed in the laboratory is distorted by the transformation Jacobian v^2/u^2 from that in the CM system, where v and u are LAB and CM velocities, respectively.[30,38] Because an electron impact ionization mass spectrometric

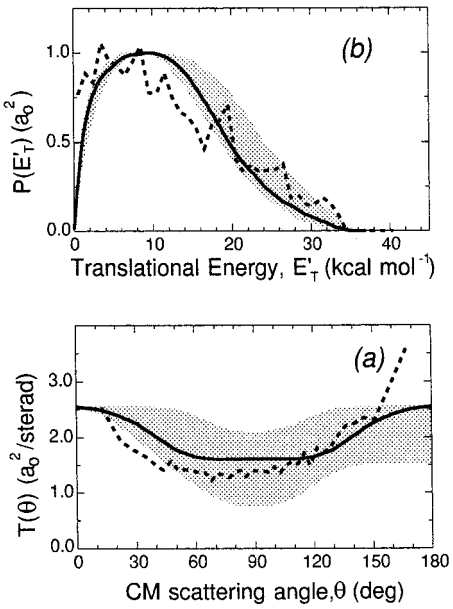

Figure 6. (a) Best-fit CM angular distribution (solid line) with error bars (hatched area) and QCT prediction (dashed line) derived at E_c = 3.8 kcal mol^{-1}. (b) Best-fit translational energy distributions (solid line) with error bars (hatched area) and QCT prediction (dashed line). The experimental results (relative units) are arbitrarily normalized to the QCT results.

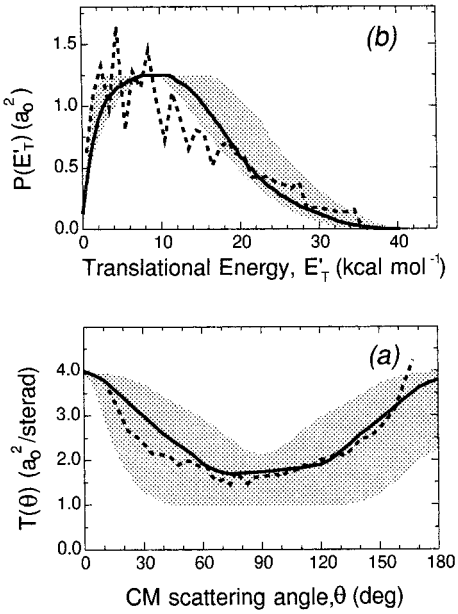

Figure 7. (a) Best-fit CM angular distribution (solid line) with error bars (hatched area) and QCT prediction (dashed line) derived at E_c = 5.1 kcal mol^{-1}. (b) Best-fit translational energy distributions (solid line) with error bars (hatched area) and QCT prediction (dashed line). The experimental results (relative units) are arbitrarily normalized to the QCT results.

detector measures the number density of products $N(\Theta)$ and not their flux, the actual relation between the LAB density and the CM flux is given by

$$N_{LAB}(\Theta,v) = I_{CM}(\theta,u)v/u^2$$

Because of the finite resolution of experimental conditions, analysis of the laboratory data is carried out, as usual, by forward convolution procedures over the experimental conditions of trial CM distributions. The final outcome is the generation of a velocity flux contour map of the reaction products, i.e., the plot of the intensity as a function of angle and velocity in the CM system, $I_{CM}(\theta,u)$. The contour map can be regarded as an *image* of the reaction.

The fit of product angular distributions and TOF spectra was achieved by a forward convolution trial-and-error procedure that assumes a separable form for the CM frame product flux distribution $I_{CM}(\theta,E'_T) = T(\theta)\ P(E'_T)$, where the $T(\theta)$ function represents the CM total differential cross section and $P(E'_T)$ is the product translational energy distribution. The energy dependence of the integral reactive cross section, as derived by QCT calculations, has been included in the data analysis; the effect was negligible, however, because of the narrow spread of relative translational energies in these experiments. The continuous lines in Figures 2−5 are the LAB angular and TOF distributions calculated from the best-fit CM angular and translational energy distributions, which are depicted a solid lines in Figures 6 and 7; the hatched areas in Figures 6 and 7 delimit the range of CM functions which still afford an acceptable fit to the data, i.e., they represent the error bars of the present determination. As can be seen in the Figures 2−5, the LAB ^{15}ND product angular and TOF distributions are well reproduced and this indicates that for this reaction the coupling between the product angular and translational energy distributions is mostly weak within the sensitivity of our data. However, in the case of the higher energy experiment, the TOF spectrum measured at $\Theta = 10°$ is somewhat faster than that derived using the best-fit functions and also shows some bimodality which is not well reproduced; an improved fit could be obtained by accounting for the coupling of $P(E'_T)$ and $T(\theta)$ and using a more energetic $P(E'_T)$ in the forward direction. This is partially true also for the spectrum taken in the backward direction (Θ = 24°). This kind of behavior is in line with what is known from simple statistical models where a larger fraction of the available energy is predicted to be released in product translation at the two poles (θ = 0° and 180°) as a mere consequence of the angular momentum conservation.[19]

The best-fit CM functions are also reported as product flux (velocity-angle) contour maps in Figure 8. The contour maps highlight the features inferred from the lab angular distributions; in fact, from them, one can immediately see how the ND angular distribution is distributed over all of the angular range with peaks at the two poles. The position of the peak in the CM velocity scale reflects the fraction of total available energy released as product translational energy and this mirrors, by energy conservation, the product internal (vibrational + rotational) energy distribution.

The average product translational energy

$$\langle E'_T \rangle = \sum_{E'_T} P(E'_T) E'_T / \sum_{E'_T} P(E'_T)$$

is 11.9 and 12.1 kcal mol^{-1} for the lower and higher energy experiment, respectively, that is, about 32% of the total available energy (the total available energy is given by the sum of the collision energy and of the reaction exothermicity). This modest fraction of energy released as translational motion of the products points to a high internal (rovibrational) excitation, as seen in spectroscopic studies.[25,27,28]

III. QCT Calculations

Standard QCT methods were used to study the N(^{2}D) + D_2 reaction on the $1^2A''$ surface of Pederson et al.[13] A maximum impact parameter b_{max} of $3.0a_0$ was used for low energies (below 4 kcal mol^{-1}) and increased to $4.0a_0$ for higher energies.

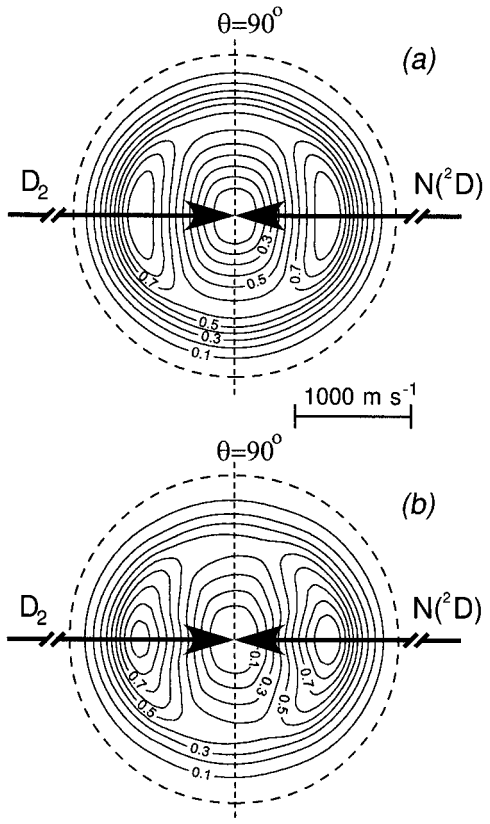

Figure 8. CM polar flux (velocity-angle) contour maps of the ND product at $E_c = 3.8$ kcal mol^{-1} (a) and $E_c = 5.1$ kcal mol^{-1} (b).

Convergence of cross sections with respect to the value of b_{max} was carefully tested. The initial atom−diatom separation was chosen to be $10a_0$ for all calculations. A fifth order Adams−Moulton predictor−corrector method was used for the trajectory calculations, using a time step of 0.1 fs. All calculations refer to the Davidson corrected version of the potentials described in ref 13. This gives product angular distributions which are essentially identical to the uncorrected surface,[20] except for an overall energy shift that arises from the 0.4 kcal mol^{-1} difference in barrier height. The calculations have considered D_2 in initial states $v = 0$ and $j = 0$, 1, and 2. These results were averaged over a rotational Boltzmann distribution in making comparison with experiment. Ten-thousand trajectories were evaluated for each energy and each reagent state.

We have neglected the influence of electronic states other than $1^2A''$ on the results. Of the five states that correlate to N(^{2}D) + H_2, only the $1^2A'$ state has a low enough barrier to be competitive with $1^2A''$. The $1^2A'$ surface was studied in ref 21, and it was found to have a C_{2v} insertion barrier that is similar to that for $1^2A''$ except that it is 1 kcal mol^{-1} higher in energy. A major difference between the two surfaces is that the $1^2A'$ surface correlates to excited NH($a^1\Delta$), so that it can only contribute to the NH($X^3\Sigma^-$) ground state by Renner−Teller induced transition to $1^2A''$. In ref 21, we demonstrated that the intersection seam between these two states is easily accessed starting from N(^{2}D) + H_2, so it is likely that the $1^2A'$ cross sections are similar to those for $1^2A''$ except for an overall shift up in energy by 1 kcal mol^{-1}. This leads to changes in the thermal rate constants for N(^{2}D) + H_2, as discussed in the Introduction. However, the effect of the $1^2A'$ surface on product state and angular distributions should be small, because the product distributions are determined by dissociation of the NH_2 intermediate, and the reaction from the $1^2A'$ state always involves formation of the same $1^2A''$ intermediate complex that is formed when $1^2A''$ is the initial state. In view of this, we have neglected the influence of $1^2A'$ in the results to be presented. To maintain a consistent comparison with past results,[13,21] we have not multiplied the results by the statistical weighting factor of $^1/_5$ that would account for the electronic degeneracy.

IV. Comparison between Scattering and QCT Results

The experimental CM angular distributions for N(^{2}D) + D_2 at $E_c = 3.8$ and 5.1 kcal mol^{-1} are shown as solid line in Figures 6a and 7a where they are compared with the QCT results (dashed lines) derived for the same collision energies. The experimental results (relative units) are arbitrarily normalized to the QCT results (atomic units). The error bars on the QCT results are approximately ±10% of the value of the cross sections.

The best-fit angular distribution at $E_c = 3.8$ kcal mol^{-1} is backward−forward symmetric, even though an angular distribution with a slight preference for forward scattering still gives an acceptable fit of the experimental data, as witnessed by the error bars (hatched area). Also, the degree of polarization (for the best-fit CM function $T(0°):T(90°):T(180°) = 1.0:0.63:1.0$) may vary by ∼20% with respect to the best-fit value. The best-fit $T(\theta)$ derived from experimental data at $E_c = 5.1$ kcal mol^{-1} is almost backward−forward symmetric, with a small propensity for forward scattering; the propensity is reinforced when considering the error bars. Also in this case, the degree of polarization may vary from the best-fit value of ∼0.4 ($T(0°):T(90°):T(180°) = 1.0:0.42:0.95$) by ∼15%.

The QCT angular distribution at $E_c = 3.8$ kcal mol^{-1} shows intensity in the whole angular range with a distinct excess in the backward direction, which is outside the statistical uncertainty of the calculations. The agreement with the experimentally derived $T(\theta)$ is more satisfactory in the case of the higher collision energy, where the QCT derived angular distribution shows a reduced preference for backward scattering, being almost backward−forward symmetric.

When considering the translational energy distributions, the agreement between experimental findings and theoretical predictions is good if we compare the average value of energy released as product translational energy (the QCT values are very similar to those experimentally derived, being 12.4 and 11.9 kcal mol^{-1} for the lower and higher collision energy experiments, respectively). Nevertheless, if we consider the detailed shape of the QCT and experimental functions (see Figures 6b and 7b), considerable differences can be noted: in both cases, the QCT functions peak at lower E'_T values, whereas the high-energy tails extend farther than the best-fit ones, which is especially true in the case of the lower energy experiment (the two factors compensate, giving about the same value of the average product translational energy derived from experiments).

The comparison between theory and experiment can be made more direct by simulating the LAB angular and TOF distributions using the QCT results of Figures 6 and 7. The QCT simulation is shown as dashed lines in Figures 2−5. As can be seen, the QCT CM functions do not generate the right forward−backward peak ratios in the LAB angular distributions: in both cases, the forward peak is not well reproduced, whereas a too high intensity is predicted for the backward peak. This is a consequence of the backward scattering preference of the QCT CM angular distributions. The simulated distributions are also slightly sharper than those experimentally determined, especially at the lower E_c. This is a direct consequence of the fact that the

QCT translational energy distributions peak at lower E'_T values than the functions derived from the experimental results. The consequence of this low energy peaking of the QCT $P(E_T')$ can also be seen in the TOF simulations (Figures 4 and 5), especially at the lower E_c: the QCT TOF distributions are somewhat slower than the experimental ones.

V. Discussion

An interesting aspect of QCT studies is that one can visualize the reactive trajectories. They revealed that N(^{2}D) approaches almost perpendicularly the H−H bond and inserts into it forming the intermediate NH_2 (Figure 1); if the initial approach is well away from perpendicular, then H_2 is able to reorient to the perpendicular direction before reaching the barrier top in the entrance channel. The lifetime of the formed NH_2 is quite short (few vibrational periods), but a significant amount of scrambling of energy among different degrees of freedom takes place, and as a result, the product vibrational and rotational excitation are substantial but only slightly hotter than what is obtained by a phase-space theory that imposes conservation of angular momentum.[39]

The QCT predictions on the new PES favoring perpendicular insertion attack are consistent with the present experimental results. Indeed, even though the observation of forward−backward symmetry in the angular distribution is not exclusively related to the formation of a long-lived complex, the high symmetry of the H−N−H intermediate, where the central N atom equally interacts with both H atoms, implies the same bond breaking probability for the two N−H bonds; the symmetry in the CM angular distributions can therefore be caused by the presence of an interconversion axis in the decomposing complex rather than by the persistence of the complex for a time long enough to lose memory of the initial approaching direction of the reactants. In both cases, the only possible intermediate which can account for the observed behavior is the one formed following N(^{2}D) insertion into the H−H bond. The formation of a bent NH_2 intermediate after the N(^{2}D) perpendicular insertion was also suggested by the absence of leaving atom isotope effect observed in the case of the reaction with HD.[27c] As a first conclusion, we can therefore state that both experimental findings and theoretical predictions on the new and more accurate PES confirm that the only reaction pathway is the one occurring through N(^{2}D) insertion, definitely ruling out the initially suggested abstraction mechanism.[25,26] QCT calculations have shown that an initial collinear approach, with the instantaneous formation of just one N−H bond and the simultaneous breaking of the H−H bond, is also possible but only at very high collision energies (10 kcal mol^{-1}). Interestingly, in the previous QCT study,[13] it was found that the DCSs switch from being backward peaked at low energy to being symmetric at higher energy, with 5.1 kcal/mol approximately marking the boundary between the two regimes. The reason for the backward preference at low collision energies seems to lie in the presence of the entrance barrier, which preferentially weights trajectories with small impact parameters. However, quantum calculations[22] on the N(^{2}D) + H_2 ($j = 0$) reaction indicate that the QCT low energy behavior is incorrect, because the QM angular distributions were nearly symmetric also at low collision energies. As mentioned in the Introduction, the apparent reason for this difference is tunneling, which makes it possible for the reaction to occur through higher impact parameters in the quantum results, leading to stronger forward scattering.

The present experimental and theoretical results help in elucidating the dynamics of insertion reactions when the intermediate complex is a highly excited triatomic molecule with few internal degrees of freedom. In this regard, it is instructive to compare the N(^{2}D) + H_2 reaction dynamics with those of the other known insertion reactions, seeking common features which could possibly permit us to draw general conclusions on this family of reactions.

If we compare it to the well-studied case of the O(^{1}D) + H_2 reaction, both differences and similarities emerge. In addition to having an intermediate with great stability, the two reactions have in common a high exoergicity, which permits the formation of excited rovibrational levels of the products NH/OH. In both cases, the vibrational distributions are hotter than the statistical ones, but the NH vibrational distribution is much closer to the statistical predictions than the OH one.[16c−g] Both QCT[13] and QM[22] calculations reproduce well the LIF vibrational distribution, which is at variance with the one determined from IR emission measurements,[28] whereas for the O(^{1}D) + H_2 reaction, none of the dynamical calculations on the available surfaces have ever reproduced the measured vibrational distributions, not even when accounting for the contribution of the excited-state surfaces,[17g] with the exception of a very recent experimental/theoretical study at low energy.[15f] If we consider the rotational distributions, the OH ones are completely inverted, peaking almost at the thermochemical limits;[16] the NH rotational distributions, instead, are broad with a nonlinear surprisal plot.[27,28] Remarkably, the NH rotational distributions have not been reproduced by dynamical calculations, which have instead derived rotational distributions strongly inverted and similar to those measured for O(^{1}D) + H_2 reactions.[13,22] The origin of this disagreement is not clear. If we consider the DCSs, a direct comparison between the two systems can be made because we have studied the reaction O(^{1}D) + D_2 at a collision energy (E_c = 5.3 kcal mol^{-1}) comparable to one of those reported here and practically under the same experimental conditions.[14b,15d] For O(^{1}D) + D_2, an asymmetric CM angular distribution was found with more intensity in the backward direction, which has been interpreted[14b,40] in terms of a direct abstraction mechanism (giving a backward scattered product angular distribution) superimposed to an insertion mechanism (giving a symmetric angular distribution). The abstraction is believed to take place along the first excited PES $^1\Pi$ (in collinear geometry), which has a barrier of 2.4 kcal mol^{-1}.[17e−h] In the case of N(^{2}D) + H_2, the competitive abstraction mechanism was not observed; this is not surprising because both the ground- and excited-state surfaces drive the reaction toward bent reaction pathways. Indeed, the $C_{\infty v}$ barriers on the ground $^2\Sigma$ and excited $^2\Pi$ state surfaces have two imaginary frequencies, which means that the linear barriers are not real saddle points and that there are no defined collinear reaction paths for both surfaces.[21] If we focus on the O(^{1}D) + H_2 reaction at low collision energies, where the second pathway is not active, more similarities with the present system can be noted because the DCSs are almost backward−forward symmetric with a slight preference for forward scattering (see for instance ref 15a, where the DCSs for the reaction O(^{1}D) + HD are reported at a collision energy of 2.05 kcal mol^{-1}).

Similarities and differences are noted also when comparing the N(^{2}D) + H_2 reaction dynamics with those of the two much less exoergic insertion reactions, C(^{1}D) + H_2 and S(^{1}D) + H_2. For these two reactions as well, the only possible reaction pathway is via insertion, because the abstraction path becomes energetically accessible only at $E_c > 9-15$ kcal mol^{-1} for C(^{1}D) + H_2[41] and at $E_c > 8$ kcal mol^{-1} for S(^{1}D) + H_2.[23] The main difference with these two systems is that at low E_c only the

ground vibrational level of the CH and SH products can be populated. Also, because of the reduced exothermicity, the two intermediates CH_2 and H_2S are thought to be more persistent, thus permitting a more complete energy randomization. Recent studies[18,19] have shown that for both reactions PST gives a reasonable description of the experimental product translational energy distributions. The CM angular distributions were found to be backward−forward symmetric from crossed-beam experiments[18,19] and also from PST calculations, although significant discrepancies were noted with respect to experimental determinations when comparing the degree of polarization of the angular distributions and the angle-specific translational energy distributions. For the S(^{1}D) + H_2 reaction, recent QCT calculations[23b] on a new PES[23a] have shown a substantial agreement with the experimental results of Lee and Liu,[18] even though some discrepancies are present, especially in the relative magnitude of the ICS derived for the various isotopic variants and the H/D branching ratio from the reaction S(^{1}D) + HD. Interestingly, from the analysis of the trajectories the lifetime of the complex was found to be longer than the rotational period (typical values for S(^{1}D) + D_2 were 1.5−2.5 ps at E_c = 2.3 kcal mol^{-1} considering the allowed range of impact parameters) which fully accounts for the almost statistical behavior. Also for this system a very high rotational excitation of the products was derived, similarly to what is observed for O(^{1}D) + H_2.

In conclusion, when reviewing the information now available for simple insertion reactions, we can only partly generalize their behavior, because many findings strongly depend on the different topology of the PES of each different system. These results indicate that the primary distinction that has to be made is between the reactions which are strongly exoergic (like O(^{1}D)/N(^{2}D) + H_2) and those which are only weakly exoergic (like C(^{1}D)/S(^{1}D) + H_2): in the latter case, the reduced exoergicity has the effect of increasing the intermediate lifetime leading to statistical behavior. The characteristic which distinguishes the title system from all the others is the presence of an entrance barrier; this aspect has been seen to affect the QCT predictions because it implies preferential weighting of small impact parameter trajectories.

VI. Conclusions

The comparison between experimental results and QCT predictions for the N(^{2}D) + D_2 reaction on the ab initio PES shows overall good agreement between experiment and theory for this prototypical insertion reaction. The small, yet meaningful, deviations between the CM product angular and translational energy distributions obtained by comparing QCT calculations and the experimental results mainly resides in a slight backward bias and a too low energy peaking, respectively, of the theoretical curves. These deviations are apparently not present in the QM results on the same PES. In fact, QM calculations[22,29] carried out for N(^{2}D) + H_2 show essentially symmetric angular distributions when the initial rotational distribution of H_2 is taken into account and a $P(E'_T)$ distribution which rises more slowly and peaks at somewhat higher energy than what QCT results indicate for N(^{2}D) + D_2. Clearly, before judging the quality of the new PES,[13] exact QM calculations on the isotopic variant N(^{2}D) + D_2 reproducing the experimental conditions and possibly including the low-lying excited-state surface are desirable. Such calculations are within current capabilities and are expected to become available in the near future;[42] this will permit to extend also to an insertion reaction the same kind of rigorous comparisons so far carried out only for abstraction reactions.[14a]

Acknowledgment. Support by the Italian Consiglio Nazionale delle Ricerche (CNR) and Ministero Università e Ricerca Scientifica (MURST-COFIN 1999) and the EC Commission through the RTN program Reaction Dynamics (contract No. HPRN-CT-1999-00007) are gratefully acknowledged. This work was also supported by NSF Grant CHE-9873892 (G.C.S., L.A.P.). P.C. wishes to acknowledge the Miller Institute for Basic Research in Science for a Visiting Miller Professorship and Dan Neumark for his hospitality at the Department of Chemistry of the University of California, Berkeley, where the writing of this paper was completed.

References and Notes

(1) Miller, J. A.; Kee, R. J.; Westbrook, C. K. *Annu. Rev. Phys. Chem.* **1990**, *41*, 345.
(2) Herbst, E. *Annu. Rev. Phys. Chem.* **1995**, *46*, 27.
(3) Lewis, B. *J. Am. Chem. Soc.* **1928**, *50*, 27.
(4) Steiner, W. *Z. Elecktrochem.* **1930**, *36*, 807.
(5) (a) Kistiakowsky, G. B.; Volpi, G. G. *J. Chem. Phys.* **1957**, *27*, 1141. (b) Kistiakowsky, G. B.; Volpi, G. G. *J. Chem. Phys.* **1958**, *28*, 665.
(6) Wright, A. N.; Winkler, C. A. *Active Nitrogen*; Academic Press: New York, 1968.
(7) (a) Marston, G.; Nesbitt, F. L.; Stief, L. J. *J. Chem. Phys.* **1989**, *91*, 3483. (b) Thorn, R. P.; Monks, P. S.; Stief, L. J.; Kuo, S. C.; Zhang, Z.; Ross, S. K.; Klemm, R. B. *J. Phys. Chem. A* **1998**, *102*, 846.
(8) (a) Donovan, R. J.; Husain, D. *Chem. Rev.* **1970**, *70*, 489. (b) Michael, J. V. *Chem. Phys. Lett.* **1980**, *76*, 129. (c) Umemoto, H.; Sugiyama, K.; Tsunashima, S.; Sato, S. *Bull. Chem. Soc. Jpn.* **1985**, *58*, 3076. (d) Umemoto, H.; Nakagawa, S.; Tsunashima, S.; Sato, S. *Bull. Chem. Soc. Jpn.* **1986**, *59*, 1449.
(9) McEwan, M. J.; Phillips, L. F. *Chemistry of the Atmosphere*, 1st ed.; Edward Arnold: London, 1975.
(10) (a) Balucani, N.; Cartechini, L.; Alagia, M.; Casavecchia, P.; Volpi, G. G. *J. Phys. Chem. A* **2000**, *104*, 5655. (b) Balucani, N.; Alagia, M.; Cartechini, L.; Casavecchia, P.; Volpi, G. G.; Sato, K.; Takayanagi, T.; Kurosaki, Y. *J. Am. Chem. Soc.* **2000**, *122*, 4443. (c) Balucani, N.; Bergeat, A.; Cartechini, L.; Casavecchia, P.; Volpi, G. G. Manuscript in preparation.
(11) (a) Umemoto, H.; Asai, T.; Hashimoto, H.; Nakae, T. *J. Phys. Chem. A* **1999**, *103*, 700. (b) Umemoto, H.; Nakae, T.; Hashimoto, H.; Kongo, K.; Kawasaki, M. *J. Chem. Phys.* **1998**, *109*, 5844.
(12) (a) Yung, Y. L. *Icarus* **1987**, *72*, 468. (b) Lara, L. M.; Lellouch, E.; Lopez-Moreno, J. J.; Rodrigo, R. *J. Geophys. Res.* **1996**, *101*, 23261.
(13) Pederson, L. A.; Schatz, G. C.; Ho, T.-S.; Hollebeek, T.; Rabitz, H.; Harding, L. B.; Lendvay, G. *J. Chem. Phys.* **1999**, *110*, 9091.
(14) (a) Casavecchia, P. *Rep. Prog. Phys.* **2000**, *63*, 355. (b) Casavecchia, P.; Balucani, N.; Alagia, M.; Cartechini, L.; Volpi, G. G. *Acc. Chem. Res.* **1999**, *32*, 503. (c) Casavecchia, P.; Balucani, N.; Volpi, G. G. *Annu. Rev. Phys. Chem.* **1999**, *50*, 347 and references therein.
(15) (a) Hsu, Y.-T.; Liu, K.; Pederson, L. A.; Schatz, G. C. *J. Chem. Phys.* **1999**, *111*, 7921. (b) Hsu, Y.-T.; Liu, K.; Pederson, L. A.; Schatz, G. C. *J. Chem. Phys.* **1999**, *111*, 7931. (c) Hermine, P.; Hsu, Y.-T.; Liu, K. *Phys. Chem. Chem. Phys.* **2000**, *2*, 581. (d) Alagia, M.; Balucani, N.; Cartechini, L.; Casavecchia, P.; van Kleef, E. H.; Volpi, G. G.; Kuntz, P. J.; Sloan, J. J. *J. Chem. Phys.* **1998**, *108*, 6698 and references therein. (e) Liu, X.; Lin, J. J.; Harich, S. A.; Yang, X. *J. Chem. Phys.* **2000**, *113*, 1325. (f) Liu, X.; Lin, J. J.; Harich, S. A.; Schatz, G. C.; Yang, X. *Science* **2000**, *303*, 1536.
(16) (a) Luntz, A. C. *J. Chem. Phys.* **1980**, *73*, 1144. (b) Smith, G. K.; Butler, J. E. *J. Chem. Phys.* **1980**, *73*, 2243. (c) Aker, P. M.; Sloan, J. J. *J. Chem. Phys.* **1986**, *85*, 1412. (d) Jurisch, G. M.; Wiesenfeld, J. R. *Chem. Phys. Lett.* **1985**, *119*, 511. (e) Cleveland, C. B.; Jurisch, G. M.; Trolier, M.; Wiesenfeld, J. R. *J. Chem. Phys.* **1987**, *86*, 3253. (f) Mikulecky, K.; Gericke, K.-H. *Chem. Phys.* **1993**, *175*, 13. (g) Huang, Y.; Gu, Y.; Liu, C.; Yang, X.; Tao, Y. *Chem. Phys. Lett.* **1986**, *127*, 432.
(17) (a) Alexander, A. J.; Aoiz, F. J.; Brouard, M.; Burak, I.; Fujimura, Y.; Short, J.; Simons, J. P. *Chem. Phys. Lett.* **1996**, *262*, 589. (b) Alexander, A. J.; Blunt, D. A.; Brouard, M.; Simons, J. P.; Aoiz, F. J.; Fujimura, Y.; Tsubouchi, M. *Faraday Discuss.* **1997**, *108*, 375. (c) Alexander, A. J.; Aoiz, F. J.; Banares, L.; Brouard, M.; Simons, J. P. *Phys. Chem. Chem. Phys.* **2000**, *2*, 571. (d) Badenhoop, J. K.; Koizumi, H.; Schatz, G. C. *J. Chem. Phys.* **1989**, *91*, 142. (e) Ho, T.-S.; Hollebeek, T.; Rabitz, H.; Harding, L. B.; Schatz, G. C. *J. Chem. Phys.* **1996**, *105*, 10472. (f) Schatz, G. C.; Papaioannou, A.; Harding, L. R.; Hollebeek, T.; Ho, T.-S.; Rabitz, H. *J. Chem. Phys.* **1997**, *107*, 2340. (g) Schatz, G. C.; Pederson, L. A.; Kuntz, P. J. *Faraday Discuss.* **1997**, *108*, 357. (h) Balint-Kurti, G. G.; Gonzalez, A. I.; Goldfield, E. M.; Gray, S. K. *Faraday Discuss.* **1998**, *110*, 169. (i) Gray, S. K.; Goldfield, E. M.; Schatz, G. C.; Balint-Kurti, G. G. *Phys. Chem. Chem. Phys.* **1999**, *1*, 1141. (j) Drukker, K.; Schatz, G. C. *J. Chem. Phys.* **1999**, *111*, 2451.

(18) (a) Lee, S.-H.; Liu, K. *J. Phys. Chem. A* **1998**, *102*, 8637. (b) Lee, S.-H.; Liu, K. *Chem. Phys. Lett.* **1998**, *290*, 323. (c) Lee, S.-H.; Liu, K. In *Advances in Molecular Beam Research and Applications*; Campargue, R. I., Ed.; Springer-Verlag: Berlin, Germany, 2000.

(19) Bergeat, A.; Cartechini, L.; Balucani, N.; Capozza, G.; Phillips, L. F.; Casavecchia, P.; Volpi, G. G.; Bonnet, L.; Rayez, J.-C. *Chem. Phys. Lett.* **2000**, *327*, 197.

(20) Alagia, M.; Balucani, N.; Cartechini, L.; Casavecchia, P.; Volpi, G. G.; Pederson, L. A.; Schatz, G. C.; Harding, L. B.; Hollebeek, T.; Ho, T.-S.; Rabitz, H. *J. Chem. Phys.* **1999**, *110*, 8857.

(21) Pederson, L. A.; Schatz, G. C.; Hollebeek, T.; Ho, T.-S.; Rabitz, H.; Harding, L. B. *J. Phys. Chem. A* **2000**, *112*, 2301.

(22) Honvault, P.; Launay, J.-M. *J. Chem. Phys.* **1999**, *111*, 6665.

(23) (a) Zyubin, A. S.; Mebel, A. M.; Chao, S. D.; Skodje, R. T. *J. Chem. Phys.* **2001**, *114*, 320. (b) Chao, S. D.; Skodje, R. T. *J. Phys. Chem. A* In press.

(24) (a) Suzuki, T.; Shihira, Y.; Sato, T.; Umemoto, H.; Tsunashima, S. *J. Chem. Soc., Faraday Trans.* **1993**, *89*, 995. (b) Umemoto, H.; Hachiya, N.; Matsunaga, E.; Suda, A.; Kawasaki, M. *Chem. Phys. Lett.* **1998**, *296*, 203.

(25) Dodd, J. A.; Lipson, S. J.; Flanagan, D. J.; Blumberg, W. A. M. *J. Chem. Phys.* **1991**, *94*, 4301.

(26) Kobayashi, H.; Takayanagi, T.; Yokoyama, K.; Sato, T.; Tsunashima, S. *J. Chem. Soc., Faraday Trans.* **1995**, *91*, 3771. (b) Takayanagi, T.; Kobayashi, H.; Tsunashima, S. *J. Chem. Soc., Faraday Trans.* **1996**, *92*, 1311. (c) Kobayashi, H.; Takayanagi, T.; Tsunashima, S. *Chem. Phys. Lett.* **1997**, *277*, 20.

(27) (a) Umemoto, H.; Matsumoto, K. *J. Chem. Phys.* **1996**, *104*, 9640. (b) Umemoto, H.; Asai, T.; Kimura, Y. *J. Chem. Phys.* **1997**, *106*, 4985. (c) Umemoto, H. *Chem. Phys. Lett.* **1998**, *292*, 594.

(28) Umemoto, H.; Terada, N.; Tanaka, K. *J. Chem. Phys.* **2000**, *112*, 5762.

(29) Honvault, P.; Launay, J.-M. To be published.

(30) Alagia, M.; Balucani, N.; Casavecchia, P.; Stranges, D.; Volpi, G. G. *J. Chem. Soc., Faraday Trans.* **1995**, *91*, 575.

(31) Casavecchia, P.; Balucani, N.; Volpi, G. G. The Chemical Dynamics and Kinetics of Small Radicals. In *Advanced Series in Physical Chemistry*; K. Liu, K., Wagner, A., Eds.; World Scientific: Singapore, 1995; Vol. 6, Chapter 9.

(32) Alagia, M.; Aquilanti, V.; Ascenzi, D.; Balucani, N.; Cappelletti, D.; Cartechini, L.; Casavecchia, P.; Pirani, F.; Sanchini, G.; Volpi, G. G. *Isr. J. Chem.* **1997**, *37*, 329.

(33) (a) Balucani, N.; Beneventi, L.; Casavecchia, P.; Stranges, D.; Volpi, G. G. *J. Chem. Phys.* **1991**, *94*, 8611. (b) Balucani, N.; Beneventi, L.; Casavecchia, P.; Volpi, G. G. *Chem. Phys. Lett.* **1991**, *180*, 34. (c) Balucani, N.; Casavecchia, P.; Stranges, D.; Volpi, G. G. *Chem. Phys. Lett.* **1993**, *211*, 469. (d) Balucani, N.; Beneventi, L.; Casavecchia, P.; Volpi, G. G.; Kruus, E. J.; Sloan, J. J. *Can. J. Chem.* **1994**, *72*, 888. (e) Alagia, M.; Balucani, N.; Casavecchia, P.; Laganà, A.; Ochoa de Aspuru, G.; van Kleef, E. H.; Volpi, G. G.; Lendvay, G. *Chem. Phys. Lett.* **1996**, *258*, 323. (f) Alagia, M.; Balucani, N.; Casavecchia, P.; Stranges, D.; Volpi, G. G.; Clary, D. C.; Kliesch, A.; Werner, H.-J. *Chem. Phys.* **1996**, *207*, 389. (g) Alagia, M.; Balucani, N.; Casavecchia, P.; Volpi, G. G. *J. Phys. Chem. A* **1997**, *101*, 6455. (h) Alagia, M.; Balucani, N.; Cartechini, L.; Casavecchia, P.; van Beek, M.; Volpi, G. G.; Bonnet, L.; Rayez, J. C. *Faraday Discuss.* **1999**, *113*, 133.

(34) (a) Alagia, M.; Balucani, N.; Cartechini, L.; Casavecchia, P.; van Kleef, E. H.; Volpi, G. G.; Aoiz, F. J.; Bañares, L.; Schwenke, D. W.; Allison, T. C.; Mielke, S. L.; Truhlar, D. G. *Science* **1996**, *273*, 1519. (b) Alagia, M.; Balucani, N.; Cartechini, L.; Casavecchia, P.; Volpi, G. G.; Aoiz, F. J.; Bañares, L.; Allison, T. C.; Mielke, S. L.; Truhlar, D. G. *Phys. Chem. Chem. Phys.* **2000**, *2*, 599. (c) Balucani, N.; Cartechini, L.; Casavecchia, P.; Volpi, G. G.; Aoiz, F. J.; Bañares, L.; Menendez, M.; Bian, W.; Werner, H.-J. *Chem. Phys. Lett.* **2000**, *328*, 500.

(35) Sibener, S. J.; Buss, R. J.; Ng, C. Y.; Lee, Y. T. *Rev. Sci. Instrum.* **1980**, *51*, 167.

(36) Pollard, J. E.; Trevor, D. J.; Lee, Y. T.; Shirley, D. A. *J. Chem. Phys.* **1982**, *77*, 4818.

(37) Sköld, K. *Nucl. Instrum. Methods* **1968**, *63*, 114.

(38) Lee, Y. T. In *Atomic and Molecular Beam Methods*; Scoles, G., Ed.; Oxford University Press: New York, 1987; Vol. 1.

(39) Fitzcharles, M. S.; Schatz, G. C. *J. Phys. Chem.* **1986**, *90*, 3634.

(40) Casavecchia, P. et al. *Faraday Discuss.* **1997**, *108*, 434.

(41) (a) Blint, R. J.; Newton, M. D. *Chem. Phys. Lett.* **1975**, *32*, 178. (b) Whitlock, P. A.; Muckerman, J. T.; Kroger, P. M. In *Potential Energy Surfaces and Dynamics Calculations*; Truhlar, D. G., Ed.; Plenum: New York, 1981.

(42) Honvault, P.; Launay, J.-M. Private communication.